Title
Accurate reconstruction of temporal correlation for neuronal sources using the enhanced dual-core MEG beamformer

Journal
NeuroImage, 56(4)

ISSN
1053-8119

Authors
Diwakar, Mithun
Tal, Omer
Liu, Thomas T
et al.

Publication Date
2011-06-01

DOI
10.1016/j.neuroimage.2011.03.042

Peer reviewed

NeuroImage 54 (2011) 253–263

Contents lists available at ScienceDirect

NeuroImage

journal homepage: www.elsevier.com/locate/ynimg

Dual-Core Beamformer for obtaining highly correlated neuronal networks in MEG

Mithun Diwakar [a,b,1], Ming-Xiong Huang [a,c,*,1], Ramesh Srinivasan [d,e], Deborah L. Harrington [a,c], Ashley Robb [c], Annemarie Angeles [c], Laura Muzzatti [a], Reza Pakdaman [a], Tao Song [a], Rebecca J. Theilmann [a], Roland R. Lee [a,c]

[a] Department of Radiology, University of California, San Diego, San Diego, CA, USA
[b] Department of Bioengineering, University of California, San Diego, San Diego, CA, USA
[c] Research and Radiology Services, VA San Diego Healthcare System, San Diego, CA, USA
[d] Department of Cognitive Sciences, University California, Irvine, Irvine, CA, USA
[e] Department of Biomedical Engineering, University California, Irvine, Irvine, CA, USA

ARTICLE INFO

Article history:
Received 16 February 2010
Revised 1 July 2010
Accepted 10 July 2010
Available online 17 July 2010

ABSTRACT

The "Dual-Core Beamformer" (DCBF) is a new lead-field based MEG inverse-modeling technique designed for localizing highly correlated networks from noisy MEG data. Conventional beamformer techniques are successful in localizing neuronal sources that are uncorrelated under poor signal-to-noise ratio (SNR) conditions. However, they fail to reconstruct multiple highly correlated sources. Though previously published dual-beamformer techniques can successfully localize multiple correlated sources, they are computationally expensive and impractical, requiring *a priori* information. The DCBF is able to automatically calculate optimal amplitude-weighting and dipole orientation for reconstruction, greatly reducing the computational cost of the dual-beamformer technique. Paired with a modified Powell algorithm, the DCBF can quickly identify multiple sets of correlated sources contributing to the MEG signal. Through computer simulations, we show that the DCBF quickly and accurately reconstructs source locations and their time-courses under widely varying SNR, degrees of correlation, and source strengths. Simulations also show that the DCBF identifies multiple simultaneously active correlated networks. Additionally, DCBF performance was tested using MEG data in humans. In an auditory task, the DCBF localized and reconstructed highly correlated left and right auditory responses. In a median-nerve stimulation task, the DCBF identified multiple meaningful networks of activation without any *a priori* information. Altogether, our results indicate that the DCBF is an effective and valuable tool for reconstructing correlated networks of neural activity from MEG recordings.

Published by Elsevier Inc.

Introduction

Magnetoencephalography (MEG) is a functional imaging modality that directly detects neuronal activity with a millisecond temporal resolution. However, since a number of different source configurations can generate the same MEG signal, assumptions must be made about the nature of the sources (source models) to uniquely localize them. A variety of MEG source-modeling methods have been put forth, yet no single technique is capable of adequately localizing highly correlated networks from noisy MEG data, without requiring *a priori* information, and faithfully reproducing their time courses. In the *lead-field-based approach*, a predefined grid of source dipoles is constructed. The MEG inverse problem is solved by computing the dipole moments of each source dipole located at each grid point (Hamalainen and Ilmoniemi, 1994). The dipole moments can then be examined to locate dipoles with greatest source power or strength, which yields the configuration of the source signal. However, the solution to the MEG inverse problem is highly under-determined as there are more unknown dipole moment parameters than number of MEG sensors. Thus, in order to obtain a unique solution, additional constraints must be imposed. In the *minimum L2-norm approach*, the source-grid solution that minimizes the total power of the dipole moments is chosen as the optimal solution (Hamalainen and Ilmoniemi, 1994). Given that this solution can be directly calculated as a regularized pseudo-inverse of the lead-field matrix or its variations, it has an extremely low computational cost and has been used in many MEG applications (Dale et al., 2000; Dale and Halgren, 2001; Marinkovic et al., 2003). The reconstructed signals also have smooth source time-courses. However, minimum L2-norm solutions have low spatial accuracy, and reconstructions tend to be spatially distributed even with truly focal generators.

The *minimum L1-norm approach* was developed to address the problem of low spatial resolution by selecting the source-grid solution that minimizes the total absolute value of the source strength. Though this approach provides better spatial resolution, the computational cost

* Corresponding author. Radiology Imaging Laboratory, Department of Radiology, University of California, San Diego, 3510 Dunhill Street, San Diego, CA 92121, USA.
E-mail address: mxhuang@ucsd.edu (M.-X. Huang).
[1] Both authors contributed equally to this work.

1053-8119/$ – see front matter. Published by Elsevier Inc.
doi:10.1016/j.neuroimage.2010.07.023

as implemented by algorithms such as magnetic current estimation (MCE) is increased because non-linear optimization and iterative steps are needed in the reconstruction (Uutela et al., 1999; Vanni and Uutela, 2000; Tesche, 2000; Stenbacka et al., 2002; Pulvermuller et al., 2003; Osipova et al., 2005; Auranen et al., 2005; Liljestrom et al., 2005). The time-courses of the generators determined by MCE also tend to contain discontinuities. To address these limitations, a *vector-based spatial–temporal analysis using a L1-minimum-norm solution* (VESTAL) was developed (Huang et al., 2006). In VESTAL, the linear relationship between sensor waveforms and source time-courses is ensured in a spatio-temporal sense for the L1-minimum-norm solution, and sources can be reconstructed that are fully correlated in time with high spatial accuracy. However, like L2-minimum-norm solutions, VESTAL requires good SNR, rendering it unsuitable for detecting weak brain networks.

The *beamformer methodology* is a spatial-filtering approach wherein the MEG sensor signal is filtered by different beams based on lead-field vectors corresponding to specific source-grid points (Robinson and Vrba, 1998; Sekihara et al., 2002a; Van Drongelen et al., 1996; Van Veen et al., 1997). Each of these operations generates a pseudo-*Z*-statistic, which can be maximized to find the most highly contributing source-grid dipoles. The beamformer method has low computational cost, although the orientation angle of each dipole must be optimized. The beamformer approach generally works well for MEG data with a low SNR. However, the conventional beamformer suppresses source-power estimates from source-grid dipoles that have highly correlated time-courses, as the method assumes that source time-courses from different generators are uncorrelated (Van Veen et al., 1997; Sekihara et al., 2002b). Variants of the beamformer method, including the *coherently combining signal-to-interference plus noise ratio* (CC-SINR) beamformer and the *constant modulus algorithm* (CMA) beamformer, address reconstruction of correlated sources, but have been met with moderate success (Kim et al., 2006; Nguyen and Ding, 1997). Likewise, the *coherent source suppression model* (CCSM) and the independently developed *nulling beamformer* (NB) accurately reconstruct correlated sources but require *a priori* information of interfering source locations. Furthermore, all sources cannot be simultaneously identified since correlated sources are suppressed to reconstruct a single source of interest (Dalal et al., 2006; Hui and Leahy, 2006; Hui et al., 2010; Quuran and Cheyne, 2010).

Brookes et al. (2007) developed a dual-beamformer approach to address the problem of identifying highly correlated generators by constructing a spatial filter from a linear combination of lead-field vectors from two source dipoles. Two source dipoles that generate a signal can be found by non-linearly optimizing the orientation angles of the two source dipoles, optimizing the weighting between the two sources, and searching over all combinations of source dipoles. This approach has a high computational cost, which greatly limits its application in practice. Furthermore, only the two source dipoles with most highly correlated time-courses are found, while other correlated source networks that may exist are not identified. To make the method more useful, Brookes et al. suggest using *a priori* information to fix the position of one of the two beams; however, this solution limits the method's application to well-understood neurobehavioral networks or requires information from other functional neuroimaging techniques (e.g., fMRI).

In the present study, we propose a new formulation of the beamformer technique that addresses many previous limitations of beamformer approaches. By using a spatial filter that contains the lead-fields of two simultaneous dipole sources (i.e., rather than the linear combination of the two as for the approach by Brookes and colleagues), our Dual-Core Beamformer (DCBF) can directly compute and obtain optimal source orientations and weights between two highly correlated sources. In effect, this renders non-linear optimization and non-linear searching for optimal orientations and weighting unnecessary, thereby reducing the computational time of the dual beamformer method and making it a much more useful MEG inverse-modeling technique. At the same time, the DCBF retains many desirable characteristics of the dual-beamformer approach proposed by Brookes et al. For example, our computer simulations demonstrate that DCBF successfully localizes dipole sources at very low SNR (SNR of 0.25), which is useful for many MEG recordings.

In the present approach, we use a modified Powell search to find the optimal pseudo-*Z*-score, which not only greatly reduces the computational time required for source localization, but also identifies other local maxima. All maxima, consisting of two sources each, are defined as pathways. With simulations, we show how such a search can find multiple pairs of correlated sources present in a single MEG data set. In a median-nerve stimulation experiment, we present how these pathways may be meaningful and are not simply a byproduct of DCBF.

Materials and methods

Conventional vector beamformer solution (general approach)

The beamformer spatial filter is a method by which the lead-field approach of MEG is used to estimate neuronal current sources in the brain. The lead-field approach states that for a given set of current dipole sources, the MEG sensor readings can be described by a linear combination of the source signals. The relationship between MEG sensor signals and source time-courses can be expressed as:

$$b(t) = G \cdot p(t) \tag{1}$$

where $p(t)$ is a $3p$ dimensional column vector of p source signals in 3 principle orientations; G is an $m \times 3p$ gain matrix, or lead-field matrix, estimated by MEG forward modeling for the MEG sensor grid; and $b(t)$ is an m dimensional column vector of m MEG sensor signals for the same temporal range.

The lead-field vector (L_p) for each of p source dipoles is defined as the three columns of G that correspond to the specific source dipole. Besides the lead-field vector, C , an $m \times m$ signal covariant matrix computed from $b(t)$, and ε , an $m \times m$ noise covariant matrix computed from noise-only MEG signal are also used to construct the beamformer (Van Veen et al., 1997). In order to compute the source power, orientation, and estimated neuronal activity for a dipole, the matrices Q and K must first be defined (Robinson and Vrba, 1998; Vrba and Robinson, 2001; Sekihara et al., 2004).

$$Q = \left(L_p^T \cdot C^{-1} \cdot L_p\right) \tag{2}$$

$$K = \left(L_p^T \cdot C^{-1} \cdot L_p\right)^{-1} \cdot \left(L_p^T \cdot \left(C^{-1} \cdot \varepsilon \cdot C^{-1}\right) \cdot L_p\right) \tag{3}$$

Q is inversely proportional to the source power. It has been shown that the optimal power may be obtained by inverting the minimum eigenvalue of Q (Sekihara et al., 2004):

$$P_{\text{opt}} = (min(eig(Q)))^{-1} \tag{4}$$

The optimal source orientation is therefore given by U_{min}, the three-component eigenvector corresponding to the minimum eigenvalue of Q (Sekihara et al., 2004):

$$O_{\text{opt}} = U_{\text{min}} \tag{5}$$

K is inversely proportional to the signal-to-noise ratio in source space. The estimated neuronal activity or pseudo-*Z*-score may be obtained by diagonalizing K with eigenvalue decomposition and inverting the smallest eigenvalue (Robinson and Vrba, 1998; Vrba and Robinson, 2001; Sekihara et al., 2004):

$$Z_{\text{opt}} = (min(eig(K)))^{-1} \tag{6}$$

Z is a measure of the signal-to-noise ratio in the source space. The reconstructed source signal from a particular dipole is given by (Sekihara et al., 2004):

$$p(t) = O_{opt} \cdot \left(P_{opt} \cdot C^{-1} \cdot L_p \cdot O_{opt}\right)^T \cdot b(t) \quad (7)$$

In essence, the beamformer is a method wherein the signal is spatially filtered by the lead-field vectors to find the source location with maximum activity using a scanning approach over a pre-specified source grid with thousands of nodes (potential source locations). In the vector formulation, the optimal source power, orientation, and pseudo-Z-score may be computed with eigenvalue analysis. In the scalar formulation, the optimal dipole orientation must first be found using a search (Robinson and Vrba, 1998; Vrba and Robinson, 2001). However, the scalar and vector beamformer formulations have been shown to be mathematically equivalent (Sekihara et al., 2004).

Previous dual beamformer solution (general approach)

The single beamformer approach, as described above, has an important limitation when spatially distinct yet temporally correlated sources are present in the MEG signal (Van Veen et al., 1997). Different modifications of the single beamformer approach attempt to compensate for this limitation (Kim et al., 2006; Nguyen and Ding, 1997; Brookes et al., 2007). Brookes et al. developed the dual beamformer approach specifically for reconstructing correlated sources. In this approach, a new lead-field vector is computed based on the linear combination of the two lead-field vectors from two particular source dipoles as follows:

$$L_{\text{dual}} = \alpha L_{\theta_1} + (1-\alpha) L_{\theta_2} \quad (8)$$

$L_{\theta 1}$ and $L_{\theta 2}$ are the lead-fields of the two source dipoles rotated to the orientations specified by θ_1 and θ_2, respectively. The relative dipole weights are specified by α, the weighting parameter. The pseudo-Z-statistic and reconstructed source signal are recovered in an identical manner to the scalar single beamformer method. However, to find the optimal pseudo-Z-score, both orientation angles and the weighting parameter α must also be optimized non-linearly. Using this method, only a single signal is recovered for both dipoles. The relative weighting of these signals can be estimated by the optimized weighting parameter α_{opt}. Due to the time-consuming nature of non-linear optimizing over these parameters, computing pseudo-Z-scores for every combination of current dipoles is not time-efficient. Thus, the use of other sources of information (e.g., fMRI) is suggested to fix one of the two dipoles in an *a priori* fashion, which reduces the computational needs of the dual-beamformer method (Brookes et al., 2007).

New dual-core beamformer approach (DCBF)

A major limitation of the dual-beamformer method proposed by Brookes and colleagues is the necessity to optimize the orientation of both beams and their relative weighting. Their approach requires non-linear optimizations which increase the computational complexity of the dual beamformer approach many-fold when compared to the single beamformer approach. In the present study, we show that the optimal orientations and weighting of both beams can be directly computed, instead of searched, by using a vector formulation of the dual beamformer approach. First, we start with lead-field vector for each dipole as an $m \times 3$ matrix expressed in a pre-defined coordinate basis with three axes. Alternatively, since MEG is insensitive to radially directed currents, the lead-field vector for each dipole can be decomposed by singular value decomposition (SVD) and expressed instead as an $m \times 2$ matrix to reduce the inverse problem to two spatial dimensions (Huang et al., 2006). Then, we define the combined lead-field vectors from both dipoles in the dual beamformer as an $m \times 6$ matrix, instead of a linear combination of two lead-fields:

$$L_{\text{dual}} = [L_1\ L_2] \quad (9)$$

The new L_{dual} is therefore a spatial filter with two cores rather than one. Such a description of the spatial filter allows eigenvalue analysis to analytically determine optimal orientations of each beam and optimal weighting between each beam. Similar to the pseudo-Z-statistic computation for the single vector beamformer in (3) and (6), we define the 6×6 matrix K_{dual}:

$$K_{\text{dual}} = \left(L_{\text{dual}}^T \cdot C^{-1} \cdot L_{\text{dual}}\right)^{-1} \cdot \left(L_{\text{dual}}^T \cdot \left(C^{-1} \cdot \varepsilon \cdot C^{-1}\right) \cdot L_{\text{dual}}\right) \quad (10)$$

By diagonalizing K_{dual} with eigenvalue decomposition and inverting the smallest eigenvalue, we obtain the best possible pseudo-Z-score for the two dipoles.

$$Z_{\text{opt}}^{\text{dual}} = \left(\min(\text{eig}(K_{\text{dual}}))\right)^{-1} \quad (11)$$

This step is an extension of the approach used in the single beamformer in (6) (Sekihara et al., 2004). We can also define a matrix analogous to Q_{dual} for the single beamformer in (2) to estimate the source powers and orientations:

$$Q_{\text{dual}} = L_{\text{dual}}^T \cdot C^{-1} \cdot L_{\text{dual}} \quad (12)$$

By diagonalizing Q_{dual} with eigenvalue decomposition, we can obtain the optimum beamformer power, the optimum orientations, and the optimum weighting of the two source dipoles as follows (Sekihara et al., 2004):

$$P_{\text{opt}}^{\text{dual}} = \left(\min(\text{eig}(Q_{\text{dual}}))\right)^{-1} \quad (13)$$

$$O_{opt}^{dual} = U_{min} \quad (14)$$

U_{min} is defined as the six-component eigenvector associated with the minimum eigenvalue of Q_{dual}. The first three elements of $O_{\text{opt}}^{\text{dual}}$ contain the optimal beam 1 weighting in the three different basis directions. The last three elements contain the optimal beam 2 weighting in its basis directions. The elements corresponding to beam 1 and the elements corresponding to beam 2 are scaled such that relative weighting between the beams is optimal. The cost of computation is low because the eigenvalue decompositions are performed on matrices (K_{dual} and Q_{dual}) with low dimensions (6 by 6). Since the DCBF is a vector formulation of the previous dual beamformer method (Brookes et al., 2007), reconstructed dipole orientations and weighting should be the same for both methods. To examine the computational efficiency (speed) resulting from directly computing orientations and weights instead of performing a non-linear search, 100 direct computations and 100 Nelder–Mead non-linear simplex searches were performed and timed.

The reconstructed time-course for the source dipoles is given by:

$$p(t) = O_{\text{opt}}^{\text{dual}} \cdot \left(P_{\text{opt}}^{\text{dual}} \cdot C^{-1} \cdot L_{\text{dual}} \cdot O_{\text{opt}}^{\text{dual}}\right)^T \cdot b(t) \quad (15)$$

$p(t)$, the source time-course, is a $6 \times t$ matrix whose first three rows comprise the time-course for the first source and whose last three rows comprise the time-course for the second source. Each row contains the component of the time-course along each axis. An assumption of signal reconstruction is that both signals are highly correlated. As a result, only one time-course is actually reconstructed.

However, this time-course is weighted appropriately to generate a time-course for each component of each source.

Since the optimal weighting, orientations, and pseudo-*Z*-statistic are computed directly, the only parameter left to optimize is the specific combination of dipoles that leads to the maximum pseudo-*Z*-score. As noted before, this can be accomplished by an exhaustive brute-force search over all possible dipole combinations (Brookes et al., 2007). In this scenario, if p is the number of dipoles, one would have to compute $p(p+1)/2$ pseudo-*Z*-scores to find the best dipole combination. To circumvent the long computational time of a brute-force search, *a priori* information can be used to fix the location of one dipole (Brookes et al., 2007). However, this method is not ideal when knowledge of sources is not widely accepted or is unavailable.

In the present study, a modified Powell search algorithm was implemented to find the best dipole combination without performing a brute-force calculation and without requiring *a priori* information. Let $[r_1, r_2]$ be the two coordinate axes on which the search is performed. The r_1 axis corresponds to the index of the first dipole in a given source grid, while r_2 corresponds to the index of the second dipole. Let the function that we are searching over be defined as:

$$f(r_1, r_2) = Z_{\text{opt}}^{\text{dual}}(r_1, r_2) \tag{16}$$

Suppose r_1^0 is a dipole picked randomly from a given source grid. The profile $f(r_1^0, r_2)$ is calculated and then maximized to find the corresponding r_2^{opt} value. Subsequently, the profile $f\left(r_1, r_2^{\text{opt}}\right)$ is calculated to find an optimized r_1 value. This process is repeated until stable $Z_{\text{opt}}^{\text{dual}}$, r_1^{opt}, and r_2^{opt} are reached. Since this search may converge to a local maximum, the process may be iterated multiple times using random initializations of dipoles. In this manner, r_1^{opt} and r_2^{opt}, or the optimal dipole combination can be reached more quickly than the brute-force method. In our reconstructions, the Powell search was also implemented with a taboo list to reduce computational time by interrupting the search every time a dipole combination that had already been traversed was selected again.

The results of all Powell search iterations (pairs of correlated sources) were saved as they are local maxima of $Z_{\text{opt}}^{\text{dual}}$. These local maxima, or pathways of cortical activation, represent different highly correlated networks that co-exist in the data.

Setup for computer simulations

Computer simulations were performed in order to examine the performance of both the dual-core spatial filter and the non-linear modified Powell search portions of the DCBF. The simulator was programmed to test up to three pairs of source dipoles under differing conditions of frequency, cross-correlation, and amplitude. The base signal for each dipole was programmed to be a simple sinusoidal wave in a specific direction. In addition, the noise simulation was programmed so that the SNR of each simulation could be chosen manually by adding uncorrelated random noise. The searchable source space was simulated with a fixed-source grid based on the gray-matter boundary obtained from a healthy subject's T1-weighted MRI using Freesurfer (Dale et al., 1999; Fischl et al., 2004) and a grid spacing of 7 mm. The boundary element method (BEM) was used for the MEG forward model calculation with the BEM mesh (5 mm mesh size) being the inner-skull surface from the MRI. In each case, SVD was used to reduce the lead-field vectors to $m \times 2$ matrices (Huang et al., 2006). In each simulation, the search was given 1000 random restarts. Performance was evaluated by average time to find the correct solution or equivalently, the number of searches required on average to find the solution.

To evaluate the performance of our reconstruction under differing levels of noise, simulations were performed with the following control conditions: 1 pair of sources, 30 Hz frequency, 100% intra-pair correlation, and 1:1 amplitude ratio for the two source dipoles. Reconstruction was evaluated at SNRs of 4.0, 3.0, 2.0, 1.0, 0.50, 0.33, and 0.25. In our simulations, we defined SNR in sensor domain as the total power of the signal divided by the total power of the noise that was added to the signal. To examine the effects of source signals containing more than one frequency component, the 0.25 SNR test condition was repeated for 1 pair of 100% correlated sources with a dominant 30 Hz component and a half-amplitude 20 Hz component. The 0.25 SNR test condition was also repeated to test DCBF performance in the presence of correlated noise at 10 Hz. Correlated noise was introduced by means of a single noise source of same amplitude oscillating at a frequency of 10 Hz throughout the entire simulation.

To evaluate the performance of our reconstruction under differing correlations within the source pair, simulations were performed with the control conditions: 1 pair of sources, 30 Hz frequency, 1:1 source amplitude ratio, and SNR of 2.0. The following intra-pair correlations were simulated as the variable condition: 86.6%, 75%, and 50%. To evaluate the performance of our reconstruction under differing source amplitudes, simulations were performed with the control conditions: 1 pair of sources, 30 Hz frequency, 100% intra-pair correlation, and SNR of 2.0. The following amplitude ratios were simulated as the variable condition: 1:1, 2:1, and 3:1. To evaluate the performance of our reconstruction in a more realistic scenario and for multiple dipoles, three source-pairs were selected with frequencies of 20 Hz, 30 Hz, and 40 Hz. Each source dipole had differing amplitudes. Each pair of dipoles was programmed with slightly different intra-pair correlations. The dipoles were also uncorrelated across pairs. The SNR was set to 0.6075.

To evaluate the performance of our reconstruction in the presence of three correlated sources, three sources were given a sinusoidal signal with a frequency of 30 Hz at a SNR of 0.25. The second and third sources were phase-shifted 22.5 degrees and 45 degrees from the first source. Activation maps were generated for the pathway with highest pseudo-*Z*-score from the formula:

$$Z_{\text{comb}} = \frac{\max(Z_1)\cdot[Z_1 - \min(Z_1)]}{\max(Z_1) - \min(Z_1)} + \frac{\max(Z_2)\cdot[Z_2 - \min(Z_2)]}{\max(Z_2) - \min(Z_2)} \tag{17}$$

Z_1contains the pair-wise pseudo-*Z*-scores for the first optimal dipole with all other dipole sources. Z_2 contains the pair-wise pseudo-*Z*-scores for the second optimal dipole with all other dipole sources. Monte Carlo simulations were used to obtain a distribution of pseudo-*Z*-scores produced by noise. A kernel-smoothed density-estimate was computed to produce a continuous distribution. Statistical significance of pseudo-*Z*-scores for all activation maps was determined by integration of the continuous distribution.

Setup for auditory steady-state MEG response

An auditory stimulus experiment was designed to test DCBF reconstruction of correlated sources in an actual MEG measurement. The experiment consisted of 200 epochs of evoked responses to a stereo test file. The test file consisted of an 1800 ms pre-stimulus noise measurement period and a 2000 ms post-stimulus period. The stimulus was a 500 Hz pure tone with a 40 Hz envelope modulated at 100% level. The intensity of the stimulus was balanced between left and right ears. The start and end of the stimulus were smoothed with a cosine roll-off to prevent any artifacts from the stimulus. Magnetic fields evoked by auditory stimulation were measured using an Elekta/Neuromag™ whole-head MEG system (VectorView) with 204 gradiometers and 102 magnetometers in a magnetically shielded room (IMEDCO-AG, Switzerland). EOG electrodes were used to detect eye blinks and eye movements. An interval of 1900 ms post-stimulus data was recorded, using 1500 ms of pre-stimulus data for noise measurement. Data were sampled at 1000 Hz and run through

MaxFilter to remove environment noise (Taulu et al., 2004; Taulu and Simola, 2006; Song et al., 2008, 2009). 188 artifact-free MEG responses were averaged with respect to the stimulus trigger. A BEM mesh of 5-mm mesh size for the subject was generated from the inner-skull surface using a set of T1 MRI images taken on a 1.5 T GE scanner. A fixed source grid with 7-mm spacing was generated from the gray-white matter boundary of the T1 image by Freesurfer. Lead-field vectors for each dipole source were reduced to $m \times 2$ matrices by ignoring the weakest orientation (Huang et al., 2006), reducing all reconstructed time-courses to two components. Registration of MRI and MEG was performed using data obtained from the Isotrack system prior to subject scanning in the MEG machine. The signal was then reconstructed using the dual-core beamformer approach coupled to the non-linear modified Powell search. Activation maps were generated in the same fashion as in (17). Source time-courses were low-pass filtered under 50 Hz to display the auditory response. Time–frequency (TF) analysis of the source time-courses with Morelet wavelets (5 cycle width) was performed between 1 and 50 Hz to identify transient and steady-state auditory responses.

Setup for right median nerve stimulation MEG response

The performance of the DCBF was further examined using human MEG responses to right median nerve stimulation. This task is widely used to study the somatosensory system and provides a useful standard for analyzing DCBF performance since the location of activated dipole sources is easily predictable. We conducted MEG recordings for this experiment on 6 healthy subjects (men, ages 20–42) as they underwent right median-nerve stimulation. All subjects signed the consent forms approved by the Institutional Review Board of the University of California at San Diego. Each subject's median nerve was stimulated using a bipolar Grass™ constant-current stimulator. The stimuli were square-wave electric pulses of 0.2 ms duration delivered at a frequency of 1 Hz. The inter-stimulus-interval (ISI) was between 800 and 1200 ms. The intensity of the stimulation was adjusted until robust thumb twitches were observed. A trigger was designed to simultaneously send a signal to the MEG for every stimulus delivery to allow averaging over evoked trials. Magnetic fields evoked by median nerve stimulation were measured using the Elekta/Neuromag™ whole-head MEG system. EOG electrodes were used to detect eye blinks and eye movements. An interval of 500 ms post-stimulus was recorded, using 300 ms of pre-stimulus data for noise measurement. Data were sampled at 1000 Hz and run through a high-pass filter with a 0.1 Hz cut-off and through MaxFilter to remove environmental noise (Taulu et al., 2004; Taulu and Simola, 2006; Song et al., 2008; Song et al., 2009). A minimum of 150 artifact-free MEG responses per subject were averaged with respect to the stimulus trigger. BEM mesh generation, source grid generation, MRI-MEG registration, and source time-course reconstruction were carried out in the same manner as in the auditory steady-state MEG response experiment. Activation maps were generated in the same fashion as in (17).

Results

Computer simulations

Computational time for obtaining the optimal dipole orientations and weights

To examine the difference in computational costs between the non-linear search approach from Brookes and colleagues and our analytical approach, we performed 100 Nelder-Mead non-linear simplex searches and 100 eigenvalue decompositions to obtain the optimal dipole orientations and optimal dipole weighting for two simulated dipoles. Non-linear searching and eigenvalue decomposition both resulted in accurate reconstruction of orientations and weighting with less than 1% difference. The average times for reconstruction were 0.0142 s and 1.4×10^{-4} s for the simplex search and the eigenvalue decomposition, respectively, resulting in a speed up of 100 times using our approach. Performing the exhausted analysis for all combinations of two-dipole pairs in a 5000 dipole-grid would take approximately 50 h using the non-linear search approach from Brookes and colleagues. In contrast, our direct computation approach based on eigenvalue decomposition would take approximately 30 min. As we show later in this section, the modified Powell approach further speeds up the analysis by bypassing the exhaustive analysis of all dipole combinations.

SNR

The results from the simulations designed to test performance under varying SNR are listed in Table 1. In each test, the dipole-pair locations reconstructed with the highest pseudo-*Z*-score were identical to the dipole-pair locations that were originally programmed with the signal. Thus, even under an SNR of 0.25, the reconstruction was able to localize the sources perfectly. Under all levels of SNR, the orientations were recovered faithfully ($0.27\% < \varepsilon < 2.56\%$). Orientation error, ε , was defined as the mean of the fractional errors of the individual dipole orientation ratios. Source amplitudes were reconstructed accurately across all levels of SNR ($6.8\% < \varepsilon < 7.2\%$). Reconstructed amplitudes were determined by finding the intensity of the Fourier transform for the reconstructed time-course at the appropriate frequency. When source dipoles contained signals of two frequencies, the accuracy of reconstructing each frequency component's amplitude was similar to the single frequency scenario ($\varepsilon_{30} = 7.24\%$, $\varepsilon_{20} = 7.70\%$). In the presence of correlated noise, source dipole locations were reconstructed accurately and quickly, though the amplitude error ($\varepsilon = 8.5\%$) and orientation error ($\varepsilon = 4.29\%$) were slightly higher. Interestingly, the average number of searches and the average time taken to find the optimum dipole pair are reduced linearly as the SNR decreases, but saturate as the SNR approaches zero ($r^2_{\text{search}} = 0.9608$; $r^2_{\text{time}} = 0.9599$).

Signal correlation

The results from the simulations designed to test performance under varying signal correlations are displayed in Table 2. In each case, the dipole pair reconstructed was identical to the original source dipoles.

Table 1
DCBF Performance under varying SNR.

SNR	Amplitude (nAm)				Reconstructed Amplitude (nAm)				Orientation ratio		Reconstructed orientation ratio		Average # Searches	Average Time (min)	Pseudo-*Z*-score
	Dipole 1		*Dipole 2*		*Dipole 1*		*Dipole 2*		*Dipole 1*	*Dipole 2*	*Dipole 1*	*Dipole 2*			
4.0	10	20	10	20	9.4	18.7	9.2	18.5	0.5	0.5	0.501	0.498	31.3	1.502	11.3
3.0	10	20	10	20	9.4	18.7	9.2	18.5	0.5	0.5	0.501	0.498	28.6	1.411	11.2
2.0	10	20	10	20	9.4	18.8	9.2	18.4	0.5	0.5	0.502	0.497	21.7	1.015	11.1
1.0	10	20	10	20	9.5	18.9	9.1	18.3	0.5	0.5	0.503	0.495	14.3	0.716	10.9
0.50	10	20	10	20	9.7	19.3	8.9	18.1	0.5	0.5	0.505	0.491	5.4	0.257	10.3
0.33	10	20	10	20	9.9	19.5	8.7	17.8	0.5	0.5	0.507	0.487	2.3	0.102	9.9
0.25	10	20	10	20	10.1	19.8	8.5	17.6	0.5	0.5	0.509	0.483	1.4	0.059	9.4

Table 2
DCBF Performance under varying source correlation.

Correlation	Amplitude (nAm)				Reconstructed amplitude (nAm)				Orientation ratio		Reconstructed orientation ratio		Average # Searches	Average Time (min)	Pseudo-Z-score
	Dipole 1		*Dipole 2*		*Dipole 1*		*Dipole 2*		*Dipole 1*	*Dipole 2*	*Dipole 1*	*Dipole 2*			
100%	10	20	10	20	9.4	18.8	9.2	18.4	0.5	0.5	0.502	0.498	21.7	1.015	11.1
86.6%	10	20	10	20	9.1	18.2	8.8	17.8	0.5	0.5	0.501	0.497	1	0.034	11.3
75.0%	10	20	10	20	8.9	17.7	8.5	17.1	0.5	0.5	0.501	0.497	1	0.033	11.0
50.0%	10	20	10	20	8.3	16.5	7.8	15.7	0.5	0.5	0.501	0.497	1	0.035	10.5

Thus, even under a correlation of only 50%, the reconstruction was able to localize the sources perfectly. The reconstructed amplitudes in each of these simulations faithfully matched the original source amplitudes $\left(\bar{\varepsilon} = 12.5\% ; \sigma\bar{\varepsilon} = 5.1\%\right)$ and became linearly more accurate as the pair correlation increased ($r^2 = 0.99905$). The reconstructed orientations also faithfully matched the original source orientations and exhibited little dependence on the correlation $\left(\bar{\varepsilon} = 0.40\% ; \sigma\bar{\varepsilon} = 0.18\%\right)$. Interestingly, the proper dipole pair was found more immediately, repeatedly, and quickly for non-perfectly correlated than perfectly correlated sources. For each non-perfectly correlated simulation, decreasing the original source correlation led to a concomitant linear decrease in the pseudo-*Z*-score ($r^2 = 0.99998$).

Source amplitude ratio

The results from the simulations designed to test performance under varying amplitude ratios within a pair of dipoles are shown in Table 3. The reconstructed amplitude ratios in each simulation closely reflect the original source amplitude ratio ($1.97\% < \varepsilon < 4.48\%$). In the reconstruction, the orientations faithfully represent the original source orientations ($0.34\% < \varepsilon < 1.63\%$). As one increases the relative amplitude ratios within each pair of dipoles from 1 to 2 to 3, the number of searches and the time required to find the dipole pair decrease linearly ($r^2_{\text{search}} = 0.908 ; r^2_{\text{time}} = 0.905$). The amplitude ratio did not affect the computed pseudo-*Z*-scores.

Three pairs of dipoles

The results for the six dipole (3 source-pair) simulation are presented in Table 4. All six sources were reconstructed in an average of 4.8 min and 143 searches. Increasing the number of correlated two-source networks in the simulation did not result in an unmanageable increase in computational time. Even with the low SNR (0.6075), differing intra-pair correlations, and differing amplitudes both inside and outside of each dipole pair, all of the dipoles were reconstructed to the proper spatial position. The three inter-pair correlations in this study were all zero. Furthermore, the twelve reconstructed amplitudes closely represented the original source amplitudes $\left(\bar{\varepsilon} = 11.32\% ; \sigma\bar{\varepsilon} = 5.67\%\right)$. Reconstruction of each source's orientation was reasonably accurate $\left(\bar{\varepsilon} = 3.16\% ; \sigma\bar{\varepsilon} = 2.22\%\right)$.

A third correlated source

Two of the three sources in the simulation were reconstructed accurately in an average of 1.03 searches and 0.04 min. As expected, the amplitudes of the reconstructed sources were suppressed by 47.29% due to the third correlated source. Fig. 1 shows the activation map of the three reconstructed sources, which was derived by combining the dipole pseudo-*Z*-scores. Red values were thresholded at $P<0.05$, and yellow values were thresholded at $P<10^{-5}$. The combined pseudo-*Z*-score for all three dipoles was significant ($P<10^{-5}$).

Applying DCBF to human auditory MEG responses

MEG data were obtained for the 500 Hz tone auditory stimulus tests (Brookes et al., 2007). All data were subsequently processed with MaxFilter (Taulu et al., 2004; Taulu and Simola, 2006; Song et al., 2008; Song et al., 2009) and the signal was reconstructed utilizing our new DCBF approach coupled with the modified Powell search restricted to inter-hemispheric searches. To enhance the SNR of the relatively weak auditory response, 188 responses were averaged. Fig. 2 displays the pseudo-*Z*-scores of the local maxima, or pathways, found by the modified Powell search algorithm. After 1000 starts, the optimum pathway had a pseudo-*Z*-score of 1.0791 ($P<1.3\times10^{-5}$), indicating that two highly correlated dipoles had been found. Out of the 3 identified pathways, this pathway was also found most often, taking an average of 1.1 searches or 0.0305 min. Fig. 3 displays the cortical activation map derived from plotting the combined correlations of each optimal dipole with all other dipoles in the brain. For both hemispheres, red values were thresholded at $P<0.05$, and yellow values were thresholded at $P<0.005$. Fig. 3 also shows that the activity is localized to Brodmann Areas 41 and 42 (primary and association auditory cortices) in both left and right hemispheres. Pathways with low pseudo-*Z*-scores localized to deep sources. Fig. 4 displays the time-courses of the transient and steady-state auditory responses. The left to right hemisphere source amplitude ratio was 1.11. Wavelet transform time–frequency (TF) analysis was performed on the reconstructed signal to identify the transient and steady-state responses. TF analysis between 4 and 12 Hz revealed a focal region of power immediately following stimulus delivery, corresponding to the auditory transient response. TF analysis of the source signal in the 32–48 Hz band indicated the presence of power throughout the entire stimulus period centered at 40 Hz, corresponding to the auditory steady-state response (Huang et al., 2004; Ross et al., 2005; Simpson et al., 2005).

Applying DCBF to human median nerve stimulation MEG responses

MEG data were obtained from six healthy subjects for the right median nerve stimulus test. Individual trials were averaged to enhance the SNR of the MEG evoked-response. All data were

Table 3
DCBF performance under varying source amplitude ratio.

Amplitude Ratio	Reconstructed amplitude ratio	Orientation ratio		Reconstructed orientation ratio		Average # searches	Average time (min)	Pseudo-Z-score
		Dipole 1	*Dipole 2*	*Dipole 1*	*Dipole 2*			
1:1	0.98	0.5	0.5	0.502	0.497	21.7	1.015	11.1
2:1	1.93	0.5	0.5	0.505	0.497	6.1	0.274	11.2
3:1	2.87	0.5	0.5	0.508	0.498	1.5	0.065	11.2

Table 4
DCBF performance with three source pairs.

Source Index	Correlation	Frequency (Hz)	Amplitude (nAm)		Reconstructed amplitude (nAm)		Orientation ratio	Reconstructed orientation ratio	Average # searches	Average time (min)	Pseudo-*Z*-score
			Direction 1	*Direction 2*	*Direction 1*	*Direction 2*					
1	92.39%	20	10	20	8.26	16.27	0.500	0.508	6.37	0.21	7.57
2	92.39%	20	15	25	13.88	23.97	0.600	0.579	6.37	0.21	7.57
3	95.11%	30	30	20	28.30	18.98	1.500	1.492	1.20	0.04	8.97
4	95.11%	30	12	8	9.77	6.90	1.500	1.415	1.20	0.04	8.97
5	96.59%	40	20	15	17.90	14.26	1.333	1.255	142.86	4.80	7.09
6	96.59%	40	10	12	8.59	10.12	0.833	0.849	142.86	4.80	7.09

subsequently processed with MaxFilter (Taulu et al., 2004; Taulu and Simola, 2006; Song et al., 2008, 2009), and spatial locations were reconstructed utilizing the DCBF approach. Fig. 5 shows the multiple pathways found by DCBF sorted according to pseudo-*Z*-score or correlation for a single representative subject (Subject #1).

The plateaus in Fig. 5 designate searches that yielded the same result multiple times, which are considered to be important pathways or networks of activation. Fig. 5 shows activation maps computed with (17) for three of these selected networks along with similar networks reconstructed from other subjects. The activation maps were computed in the same manner as for the auditory-response analysis. All subjects had a common network of activation in the primary somatosensory cortex (S1, including Brodmann Areas 1, 2, and 3) and the secondary somatosensory cortex (S2) (Fig. 6a). Three subjects showed common networks involving the primary somatosensory cortex (S1) and Brodmann Area 5 of the posterior parietal lobe (Fig. 6b). Three subjects also had a common network of activation involving the primary motor cortex (M1) and parts of the somatosensory cortex (S1 or S2) (Fig. 6c). Two subjects showed a previously observed network of activation involving the primary somatosensory cortex (S1) and the temporal-parietal junction, a polysensory area (Huang et al., 2006).

Discussion

In the present study, we implemented a novel and powerful dual-beamformer method that was paired with the modified-Powell search to create the DCBF. Our DCBF approach addressed various shortcomings of the earlier dual-beamformer method, the CCSM, and the NB. Instead of using a spatial filter or lead-field vector consisting of a linear combination of lead-field vectors from two dipoles, we chose to concatenate the lead-field vectors from the two dipoles together, which simultaneously covered two spatial locations at once. We were also able to perform eigenvalue decomposition and analysis of the low-dimensional *K* matrix to analytically find the optimal pseudo-*Z*-score of two dipoles directly, without having to search for their best orientations non-linearly. In addition, we performed eigenvalue decomposition of another low-dimensional *Q* matrix to analytically recover the most favorable weighting between dipoles and the best orientation of the dipoles that optimized the pseudo-*Z*-score (Sekihara et al., 2004) without the need for a time-consuming non-linear search process that takes approximately 100 times longer. Optimal source dipoles were found by our modified non-linear Powell search instead of through exhaustive brute-force search, which is about three times slower. The Powell search also enabled analysis without *a priori* information about any of the dipole positions. Thus, we were able to identify multiple highly correlated neuronal networks that were associated with meaningful local maxima of pseudo-*Z*-scores.

We conducted a series of computer simulations to test the robustness and performance of the DCBF with regards to variations in several important parameters. We showed that decreased SNR

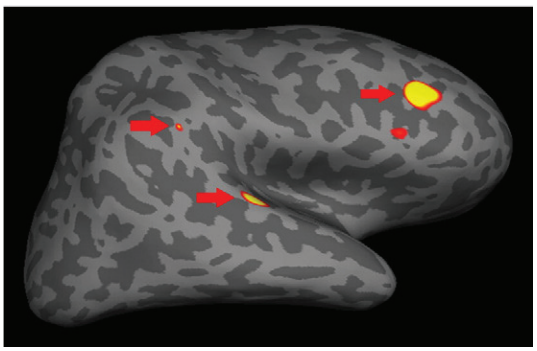

Fig. 1. Activation map for three correlated sources. The red arrows on the activation map indicate the position of the three source dipoles. The map was thresholded such that red indicates $P<0.05$ and yellow indicates $P<10^{-5}$.

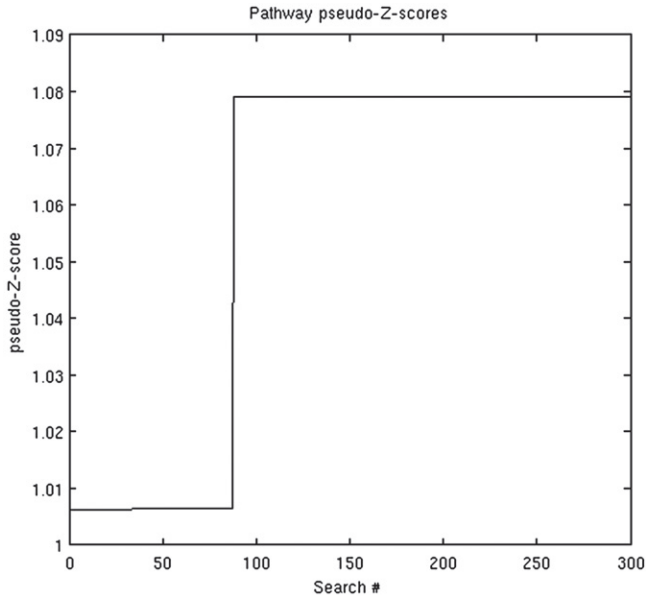

Fig. 2. Stereo auditory stimulation in a human subject: pathways with associated pseudo-*Z*-scores. Plateaus in the plot denote searches that yielded the same result (local maximum) multiple times. Results that were found multiple times were considered important pathways. Only 300 out of 1000 searches are shown to emphasize the transition between pathways. The pathway with maximum correlation (pseudo-*Z*-score) and maximum size involved both primary auditory cortices. Its activation map is depicted in Fig. 3.

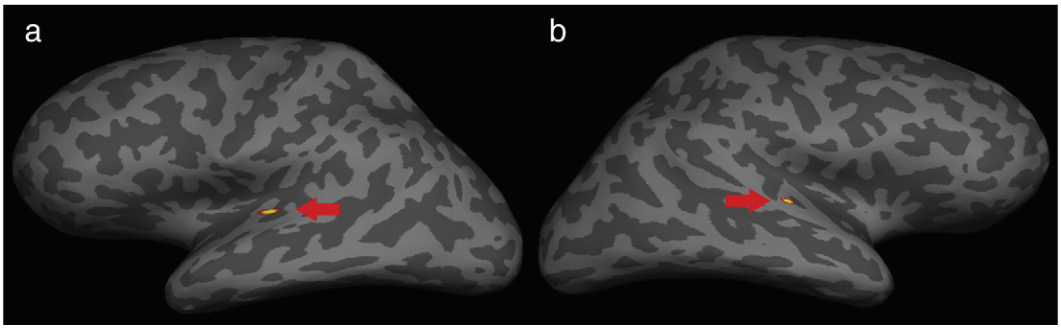

Fig. 3. Cortical activation map during stereo auditory-stimulation. Left hemisphere: The cortical activation map shows activation in the left primary auditory cortex. a. Right hemisphere: The cortical activation map shows activation in the right primary auditory cortex. Red regions were thresholded at $P<0.05$ and yellow regions were thresholded at $P<0.005$.

leads to faster localization of the source dipoles during the modified Powell search. A Powell search has the best probability of finding peaks with broad bases. Thus, we believe that lower SNR leads to a broader peak in pseudo-*Z*-score, which allows the optimal dipole combination to be identified more readily. In fact, the reconstruction performed reliably even under conditions of 0.25 SNR for both single

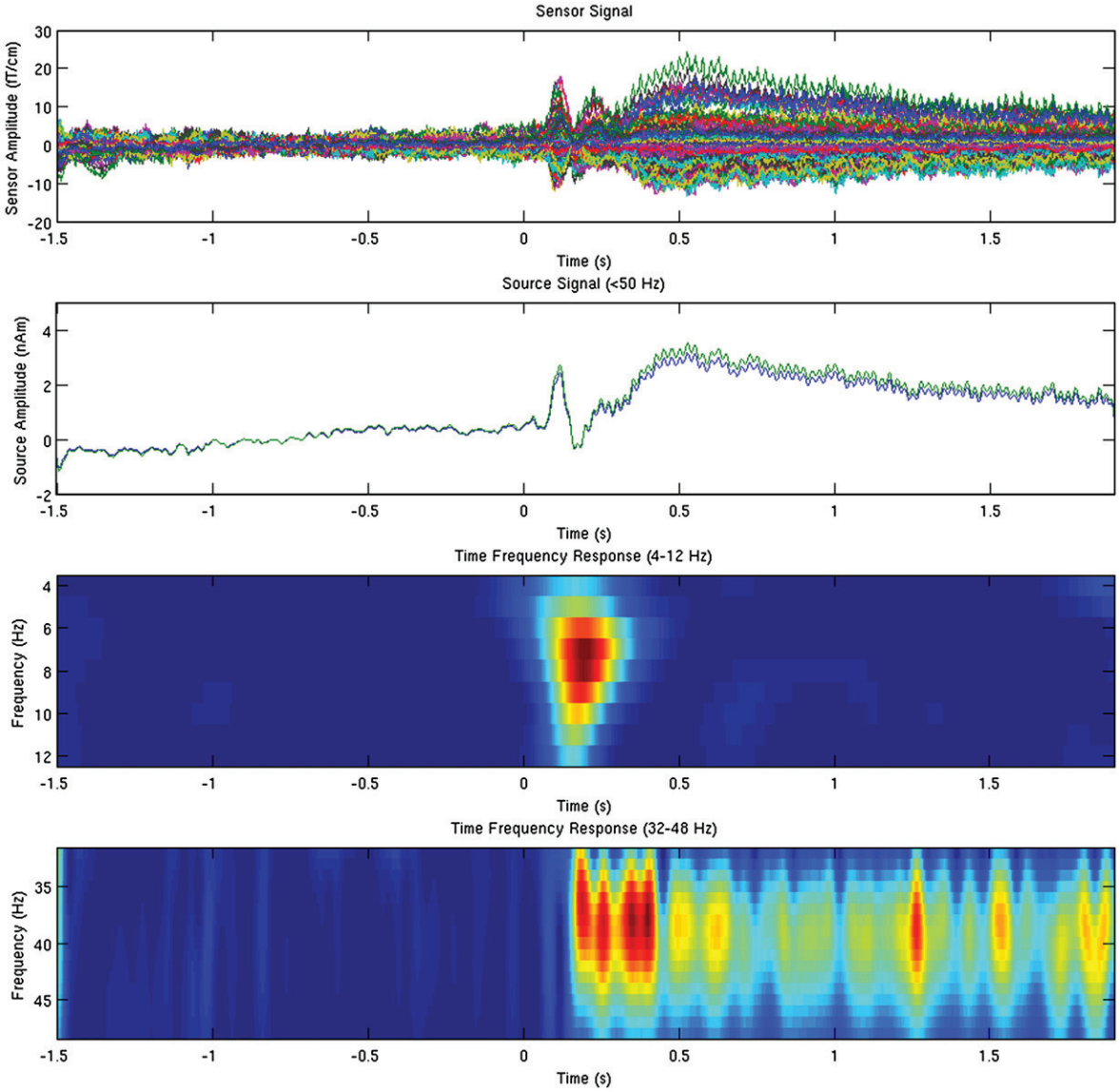

Fig. 4. Stereo auditory-stimulation signal time-courses. The top panel shows the averaged sensor waveform for the auditory response. The second panel shows the auditory response for both right hemisphere (blue) and left hemisphere (green). The third panel shows the transient auditory-response between 4 and 12 Hz with time–frequency analysis. The fourth panel shows the steady-state auditory centered at 40 Hz with time–frequency analysis.

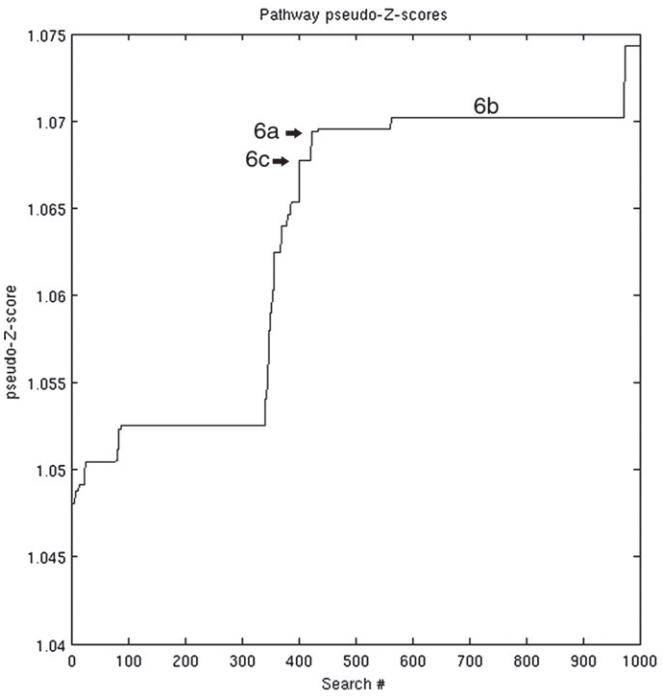

Fig. 5. Right median-nerve stimulation for human subject #1: pathways with associated pseudo-*Z*-scores. Plateaus in the plot above denote searches that yielded the same result (local maximum) multiple times. Results that were found multiple times were considered important pathways. Fig. 6 depicts the activation maps of selected pathways for subject #1 and other subjects.

and dual frequency sources and for both uncorrelated and correlated band-limited noise. At every SNR tested, our reconstruction technique successfully located the source dipoles without error. For spontaneous recordings, the MEG signal can often have a very low SNR, especially since the data cannot be averaged. For evoked recordings, a higher SNR can be obtained from averaging. Our computer simulations show that the DCBF may be applied for both types of recordings, since the method operates over a wide range of SNR.

By varying source correlation, we found that the DCBF successfully identified sources even when their signals were only 50% correlated. In fact, non-purely correlated sources were localized much more quickly than 100% correlated sources because the pseudo-*Z*-score solution space is less sharply peaked around the global maximum for non-purely correlated sources than for fully correlated sources.

To test the performance of our direct computation of optimal dipole weighting, we performed computer simulations with source dipoles emitting signals at varying ratios of amplitudes. Interestingly, as we increased the disparity in amplitude between signals, the reconstruction was able to localize the source dipoles more quickly. Differing source amplitudes likely led to a broader peak in pseudo-*Z*-score, allowing the optimal dipole combination to be identified more readily. The primary purpose of the amplitude simulations, however, was to examine if the reconstructed signals still maintained the proper amplitude weighting. Reconstructed amplitude ratios were indeed quite close to the original source amplitude ratios, confirming that our approach to obtaining optimal weighting was successful.

To determine whether the DCBF could perform in real-world conditions, we designed one simulation with three pairs of non-purely correlated dipoles. All three pairs of correlated sources were localized accurately within an average of 5 min. Furthermore, the amplitude ratios and orientations were reconstructed with only minor error, demonstrating that the DCBF can accurately reconstruct multiple simultaneously activated networks of correlation.

Another simulation was designed at low SNR to test the ability of the DCBF to reconstruct three correlated dipoles. Only two sources could be located with the Powell search, and their amplitudes were suppressed. The suppression occurred due to the underlying assumption that only two sources are correlated. Thus, the effect was similar to suppression of the conventional single beamformer in the presence of a second correlated source. However, the generated activation map shows that the DCBF successfully localized all three correlated-source in a significant manner (Fig. 1).

By applying our novel method to the analysis of bilateral auditory-stimulation data in humans, we showed that the DCBF could quickly (< 20 s) and accurately reconstruct correlated sources in a real experiment. Analysis of the pathway most frequently found and with highest pseudo-*Z*-score revealed sources located in the primary auditory cortices, as expected. In addition, time–frequency analysis of the reconstructed signal showed both the expected 40 Hz steady-state response and the transient response.

To explore the idea of finding multiple networks, we also applied the DCBF approach in an analysis of right median-nerve stimulation data from six healthy subjects. A plot of the number of searches as a function of pseudo-*Z*-scores showed different local maxima that were found multiple times, indicating the presence of different pathways. We found that the most common pathway among subjects corresponded to activation in the primary somatosensory area (S1, including BA 1, 2, and 3) and the secondary somatosensory area (S2). Two other pathways identified in half of the subjects included S1 and a classic sensory-transduction area (Brodmann Area 5), and S1 or S2 and the dorsal aspect of the primary motor area (M1). The activations in S1, S2, and M1 evoked by median-nerve stimuli are well-documented by MEG (see review in Huang et al., 2000a,b, 2005).

Summary

The most important features of the DCBF approach arise from incorporating the lead-field vectors of two simultaneously activated neuronal sources into a single spatial filter. With this novel beamformer, we were able to successfully compute optimal dipole weights, orientations, and pseudo-*Z*-scores, eliminating time-consuming searches that hindered the previous dual-beamformer approach. In addition, by utilizing a powerful Powell search with a taboo list, we were able to reconstruct optimal source dipoles quickly without the use of *a priori* information. The changes and optimizations we made decreased the total computing time from tens of hours (Brookes et al., 2007) to less than 15 min, making the DCBF a viable and useful MEG source localization method for correlated sources. Future directions include extending the DCBF framework to three or four beams to find tightly correlated and complex networks of activity. The DCBF can also be migrated from a time-domain analysis to a frequency domain or time–frequency (wavelet) domain analysis to reduce the effects of noise and phasing.

Acknowledgments

This work was supported in part by a research grant from the McDonnell Foundation (220020185) via the Brain Trauma Foundation (PI: Jamshid Ghajar, site PIs: Lee and Huang), Merit Review Grants from the Department of Veterans Affairs to Huang (051455 and 060812), Lee (E4477-R), and Harrington (1IO1CX000146-01 and B501R), and from the NIH to Srinivasan (R01-MH068004) and to Shu Chien (5T32HL007089-34). We would also like to thank Jamshid Ghajar for his encouragement and support and Omer Tal for many helpful discussions. In addition, we would like to thank three anonymous reviewers' constructive suggestions that substantially strengthened the present study.

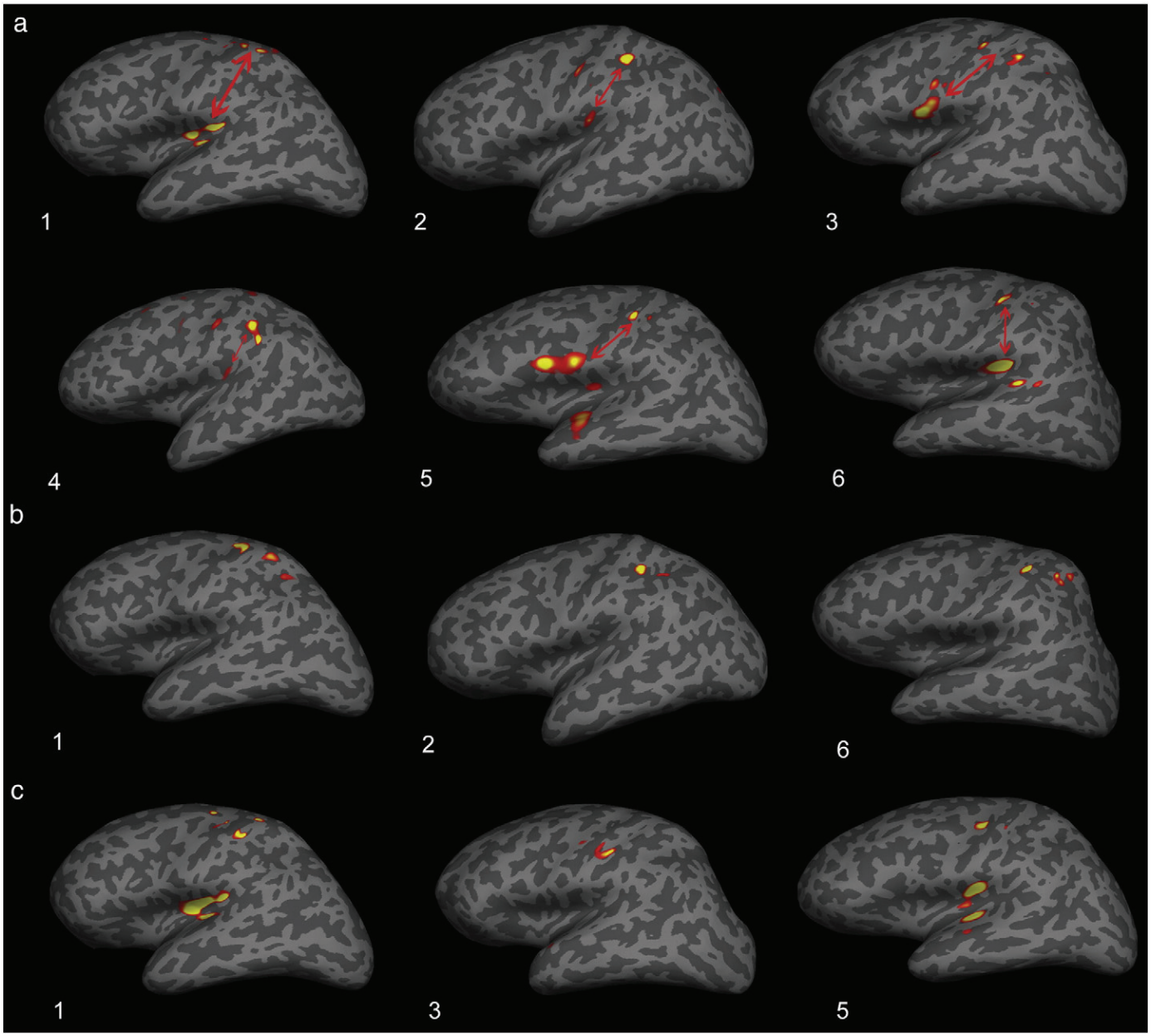

Fig. 6. Right median-nerve stimulation activation maps for six human subjects. Pathway 6a—Activity in primary somatosensory area (S1) and secondary somatosensory area (S2) (shown with red arrows). Pathway 6b—Activity in S1 and somatosensory association cortex (Brodmann Area 5). Pathway 6c—Activity in S1 and/or S2 and the dorsal aspect of the primary motor area (M1). Red regions were thresholded at $P<0.05$ and yellow regions were thresholded at $P<0.001$. Subject ID numbers are shown to the bottom-left of each cortical map.

References

Auranen, T., Nummenmaa, A., Hamalainen, M.S., Jaaskelainen, I.P., Lampinen, J., Vehtari, A., Sams, M., 2005. Bayesian analysis of the neuromagnetic inverse problem with l(p)-norm priors. Neuroimage 26, 870–884.

Brookes, M.J., Stevenson, C.M., Barnes, G.R., Hillebrand, A., Simpson, M.I.G., Francis, S.T., Morris, P.G., 2007. Beamformer reconstruction of correlated sources using a modified source model. Neuroimage 34, 1454–1465.

Dalal, S.S., Sekihara, K., Nagarajan, S.S., 2006. Modified beamformers for coherent source region suppression. IEEE Trans. Biomed. Eng. 53, 1357–1363.

Dale, A.M., Halgren, E., 2001. Spatiotemporal mapping of brain activity by integration of multiple imaging modalities. Curr. Opin. Neurobiol. 11, 202–208.

Dale, A.M., Fischl, B., Sereno, M.I., 1999. Cortical surface-based analysis: I Segmentation and surface reconstruction. Neuroimage 9, 179–194.

Dale, A.M., Liu, A.K., Fischl, B.R., Buckner, R.L., Belliveau, J.W., Lewine, J.D., Halgren, E., 2000. Dynamic statistical parametric mapping: combining fMRI and MEG for high-resolution imaging of cortical activity. Neuron 26, 55–67.

Fischl, B., van der, K.A., Destrieux, C., Halgren, E., Segonne, F., Salat, D.H., Busa, E., Seidman, L.J., Goldstein, J., Kennedy, D., Caviness, V., Makris, N., Rosen, B., Dale, A.M., 2004. Automatically parcellating the human cerebral cortex. Cereb. Cortex 14, 11–22.

Hamalainen, M.S., Ilmoniemi, R.J., 1994. Interpreting magnetic fields of the brain: minimum norm estimates. Med. Biol. Eng. Comput. 32, 35–42.

Huang, M., Aine, C., Davis, L., Butman, J., Christner, R., Weisend, M., Stephen, J., Meyer, J., Silveri, J., Herman, M., Lee, R.R., 2000a. Source on anterior and posterior banks of the central sulcus identified from magnetic somatosensory evoked responses using multi-start spatio-temporal localization. Hum. Brain Mapp. 11 (2), 59–76.

Huang, M.X., Aine, C., Davis, L., Butman, J., Christner, R., Weisend, M., Stephen, J., Meyer, J., Silveri, J., Herman, M., Lee, R.R., 2000b. Sources on the anterior and posterior banks of the central sulcus identified from magnetic somatosensory evoked responses using multistart spatio-temporal localization. Hum. Brain Mapp. 11, 59–76.

Huang, M.X., Harrington, D.L., Paulson, K.M., Weisend, M.P., Lee, R.R., 2004. Temporal dynamics of ipsilateral and contralateral motor activity during voluntary finger movement. Hum. Brain Mapp. 23, 26–39.

Huang, M.X., Lee, R.R., Miller, G.A., Thoma, R.J., Hanlon, F.M., Paulson, K.M., Martin, K., Harrington, D.L., Weisend, M.P., Edgar, J.C., Canive, J.M., 2005. A parietal-frontal network studied by somatosensory oddball MEG responses, and its cross-modal consistency. Neuroimage 28, 99–114.

Huang, M., Dale, A.M., Song, T., Halgren, E., Harrington, D.L., Podgorny, I., Canive, J.M., Lewis, S., Lee, R.R., 2006. Vector-based spatial–temporal minimum L1-norm solution for MEG. Neuroimage 31, 1025–1037.

Hui, H.B., Leahy, R.M., 2006. Linearly constrained MEG beamformers for MVAR modeling of cortical interactions. 3rd IEEE International Symposium on Biomedical Imaging: Nano to Macro, 2006, pp. 237–240.

Hui, H.B., Pantazis, D., Bressler, S.L., Leahy, R.M., 2010. Identifying true cortical interactions in MEG using the nulling beamformer. Neuroimage 49, 3161–3174.

Kim, S., Lee, C., Kang, H., 2006. Optimum beamformer in correlated source environments. J. Acoust. Soc. Am. 120 (6), 3770–3781.

Liljestrom, M., Kujala, J., Jensen, O., Salmelin, R., 2005. Neuromagnetic localization of rhythmic activity in the human brain: a comparison of three methods. Neuroimage 25, 734–745.

Marinkovic, K., Dhond, R.P., Dale, A.M., Glessner, M., Carr, V., Halgren, E., 2003. Spatiotemporal dynamics of modality-specific and supra-modal word processing. Neuron 38, 487–497.

Nguyen, T., Ding, Z., 1997. CMA beamforming for multipath correlated sources. IEEE Int. Conf. Acoust. Speech Signal Process. 3, 2521–2524.

Osipova, D., Ahveninen, J., Jensen, O., Ylikoski, A., Pekkonen, E., 2005. Altered generation of spontaneous oscillations in Alzheimer's disease. Neuroimage 27, 835–841.

Pulvermuller, F., Shtyrov, Y., Ilmoniemi, R., 2003. Spatiotemporal dynamics of neural language processing: an MEG study using minimum-norm current estimates. Neuroimage 20, 1020–1025.

Quuran, M.A., Cheyne, D., 2010. Reconstruction of correlated brain activity with adaptive spatial filters in MEG. Neuroimage 49, 2387–2400.

Robinson, S., Vrba, J., 1998. Functional neuroimaging by synthetic aperture magnetometry. In: Yoshimoto, T., Kotani, M., Kuriki, S., Karibe, H., Nakasato, N. (Eds.), Recent advances in biomagnetism. Tohoku Univ. Press, Sendai, pp. 302–305.

Ross, B., Herdman, A.T., Pantev, C., 2005. Right hemispheric laterality of human 40 Hz auditory steady-state responses. Cereb. Cortex 15 (12), 2029–2039.

Sekihara, K., Nagarajan, S., Poeppel, D., Marantz, A., 2002a. Performance of an MEG adaptive-beamformer technique in the presence of correlated neural activities: effects on signal intensity and time course estimates. IEEE Trans. Biomed. Eng. 49 (12), 1534–1546.

Sekihara, K., Nagarajan, S., Poeppel, D., Marantz, A., Miyashita, Y.M., 2002b. Application of an MEG eigenspace beamformer to reconstructing spatio-temporal activities of neural sources. Hum. Brain Mapp. 15, 199–215.

Sekihara, K., Nagarajan, S., Poeppel, D., Marantz, A., 2004. Asymptotic SNR of scalar and vector minimum-variance beamformers for neuromagnetic source reconstruction. IEEE Trans. Biomed. Eng. 51 (10), 1726–1733.

Simpson, M.I.G., Hadjipapas, A., Barnes, G.R., Furlong, P.L., Witton, C., 2005. Imaging the dynamics of the auditory steady-state evoked response. Neurosci. Lett. 16 (3), 195–197.

Song, T., Gaa, K., Cui, L., Feffer, L., Lee, R.R., Huang, M.X., 2008. Evaluation of signal space separation via simulation. Med. Biol. Eng. Comput. 46, 923–932.

Song, T., Cui, L., Gaa, K., Feffer, L., Taulu, S., Lee, R.R., Huang, M.X., 2009. Signal space separation algorithm and its application on suppressing artifacts caused by vagus nerve stimulation for magnetoencephalography recordings. J. Clin. Neurophysiol. 26 (6), 392–400.

Stenbacka, L., Vanni, S., Uutela, K., Hari, R., 2002. Comparison of minimum current estimate and dipole modeling in the analysis of simulated activity in the human visual cortices. Neuroimage 16, 936–943.

Taulu, S., Simola, J., 2006. Spatiotemporal signal space separation method for rejecting nearby interference in MEG measurements. Phys. Med. Biol. 51, 1759–1768.

Taulu, S., Kajola, M., Simola, J., 2004. Suppression of interference and artifacts by the signal space separation method. Brain Topogr. 16, 269–275.

Tesche, C., 2000. Evidence for somatosensory evoked responses in human temporal lobe. NeuroReport 11, 2655–2658.

Uutela, K., Hamalainen, M., Somersalo, E., 1999. Visualization of magnetoencephalographic data using minimum current estimates. Neuroimage 10, 173–180.

Van Drongelen, W., Yuchtman, M., Van Veen, B.D., Van Huffelen, A.C., 1996. A spatial filtering technique to detect and localize multiple sources in the brain. Brain Topogr. 9 (1), 39–49.

Van Veen, B.D., Van Drognelen, W., Yuchtman, M., Suzuku, A., 1997. Localisation of brain electrical activity via linearly constrained minimum variance spatial filtering. IEEE Trans. Biomed. Eng. 44 (9).

Vanni, S., Uutela, K., 2000. Foveal attention modulates responses to peripheral stimuli. J. Neurophysiol. 83, 2443–2452.

Vrba, J., Robinson, S.E., 2001. Signal processing in magnetoencephalography. Methods 25 (2), 249–271.